GENERAL AND APPLIED PHYSICS

Design and Analysis of All-Optical Isolator Based on Linear Photonic Crystal

Kamanashis Goswami[1] · Haraprasad Mondal[1,2] · Mrinal Sen[1] · Anup Sharma[2]

Abstract

In essence of fundamental challenges faced by optical industry, it is quite arduous to achieve all optical isolator. It has become urgent for optical communication to meet the demand of fast-moving digital world. A new T-shaped design of an all-optical isolator, based on square lattice (rods in air) of two-dimensional photonic crystal (PhC) structure, has been proposed. The proposed isolator operates on the principle of optical beam interference within the waveguides. The bias signal is capable to make the device function as an all-optical isolator by interfering with signals coming from input as well as output ports. The performance of the projected device has been analyzed and several performance metrics have been calculated. Plane wave expansion (PWE) and finite difference time domain (FDTD) methods have been used to calculate the band structure and to analyze the device performances by observing electric field distribution, respectively. The simulation results show the high contrast ratio of ~ 10 dB at worst case scenario. Owing to its simple with ultra-compact footprint (131 μm^2) and high contrast ratio altogether make the device practicable for future generation on chip photonic integrated circuits.

1 Introduction

In last couple of decades, a massive development in the field of electronics, ranging from a digital calculator to quantum computers [1], has been observed. In the recent years, data communication [2] has been focused in the timeline and it has deep impact on our day to day lives. Due to the growing demand of data communication (from astronomy [3, 4] to light detection and ranging (LiDAR) [5, 6] in automobile), the need to develop compact and ultra-fast system has been

✉ Haraprasad Mondal
mandal.haraprasad@gmail.com

✉ Mrinal Sen
mrinal.sen.ahm@gmail.com

Kamanashis Goswami
kamanashis.goswami@gmail.com

Anup Sharma
anupnewsmail@gmail.com

[1] Electronics Engineering, Indian Institute of Technology (ISM), Dhanbad, Jharkhand, India

[2] Institute of Engineering and Technology, Dibrugarh University, Dibrugarh University, Dibrugarh, Assam 786001, India

increased exponentially. Here, the term photonic integrated circuit (PIC) [7–9] comes to meet the demand of the folks who are technology evangelist. Moreover, researchers are engaging themselves to explore the field of photonics to make possible "more than Moore" [10–15]. However, to operate the electronic component, the electricity is used; on contrary, photonics integrated circuits (PICs) use light to operate its components [16]. As a result, PICs offers ultra-compact footprint area (which is in micrometer scale), high power optimization, low heat dissipation/low thermal losses, large integration capacity, and compatibility with existing process flow that allow for high profit, volume manufacturing, and lower prices . Primarily, PICs are divided into linear [17–19] and nonlinear domain [20, 21]. The linear PICs offer higher bandwidth with low operating power whereas nonlinear PICs need higher operating power and offers narrow operating band width domain. In recent past, several optical devices in linear domain like AND gate [22–25], de-mux [26, 27], decoder [28–33], filter [34, 35], coupler [36], polarizer [37], and adder/subtractor [38–41] have been reported. However, optical communication/PICs consist of three major sections, namely source, detector, and communicating medium/optical devices. An active source (like LASER and LED) is very phase-sensitive and it is needed to be protected

from any other undesired optical signal. The solution to this limitation can be overcome by an optical circuit, called as optical isolator [42, 43]; very often, it is known as optical diode, which allows the light to flow in unidirectionally; i.e., it prevents optical signal from reflecting back toward the source. Thereafter, it eliminates the noise generation or any interferences. Therefore, it is highly recommended to incorporate an optical isolator circuit in any high-end future generation optical processors. In this context, few optical isolator circuits based on several techniques have already been reported. For example, J. Fujita et al. [44] have proposed a polarization-independent optical isolator based on a Mach–Zehnder interferometer, where they achieved the extinction ratio of 19 dB but having an excess loss of 2 dB at 1.54 μm operating wavelength. Moreover, the reported device has a bulky dimension of more than 8.0 mm. Similarly, another polarization-independent Mach–Zehnder interferometer-based optical isolator circuit has been reported by Zhuromskyy et al. [45] where they have eliminated the requirement of TM/TE phase matching, hence, making the device suitable for fabrication. On the other hand, Sahoo et al. [46] have proposed a novel design of an optical isolator on two-dimensional photonic crystal-based nonlinear ring resonator. The device works based on asymmetrical coupling between waveguide and ring resonator by changing its operating frequency for forward and backward direction using Kerr effect. They have achieved a contrast ratio of 57% for backward and forward propagation. Moreover, E. N. Bulgakov et al. [47] have proposed L-shaped optical diode which is based on one nonlinear Kerr micro cavity with two dipole modes. Different coupling of the dipole modes makes the structure asymmetric. With the help of input signal power or input signal frequency, the direction of the diode is controlled. In same line, Rostamia [48] has proposed a nonlinear optical isolator (piecewise linear) based on array of two-port nonlinear ring resonators. The coupling coefficient and ring length have been used for controlling the threshold and the slope of linear part. The device offers 30 dB isolation at the frequency of 3 THz and insertion loss less than 1 dB. The footprint of the device is reported as 0.2 mm^2. Additionally, Chen Wang et al. [49] have projected linear silicon PhC slab heterojunction isolator having slab thickness of 200 nm. Their reported device has forward transmissivity greater than two order round trip transmissivity for the in-plane infrared light across the structure at the wavelength and bandwidth of 1550 nm and 50 nm, respectively.

The above limitations of the reported isolator have motivated authors to design an optical isolator in linear optical domain. In this context, an optical isolator based on purely linear photonic crystal platform has been proposed in this paper. The light beam interference phenomena have been exploited for the operation of the proposed isolator. A 180-degree phase shifter has been introduced in the input–output waveguide which plays the key role to make constructive/destructive interference between input/output signal and bias signal.

The rest portions of the article are arranged by maintaining a sequence, which are as follows. In Sect. 2, the detail design procedure of the proposed optical isolator has been discussed. Moreover, the band diagram of the photonic crystal in non-defect mode as well as guided band diagram of the defect mode of the photonic crystal has been presented in the same section. Followed by design procedure, the simulation results of the proposed device have been analyzed in Sect. 3. Few performance metrices have also been discussed in the same section. Finally, the conclusion of the proposed work has been written in the last section of the article.

2 Architectural Design of the Device

Here, the schematic design of the proposed optical isolator and band diagram of the photonic crystal structure (where the proposed device has been designed) have been discussed in details. A two-dimensional, rods-in-air of square lattice PhC platform has been chosen to design the proposed isolator.

The device is composed of an array of 25×18 silicon (Si) rods with lattice constant (a) of 540 nm, which is equivalent to foot print of 131 μm^2. The refractive index of the silicon rods and their radius are considered to be 3.46 and 120 nm, respectively. The proposed isolator is having two waveguides (which are formed by removing rods in Γ-X direction of PhC); the horizontal waveguide is used for propagation of input and output signals whereas the vertical waveguide is used for bias signal, as shown in the Fig. 1. The vertical waveguide meets the horizontal waveguide at a junction and forms a T-shaped structure. Moreover, a π-phase shifter [50]
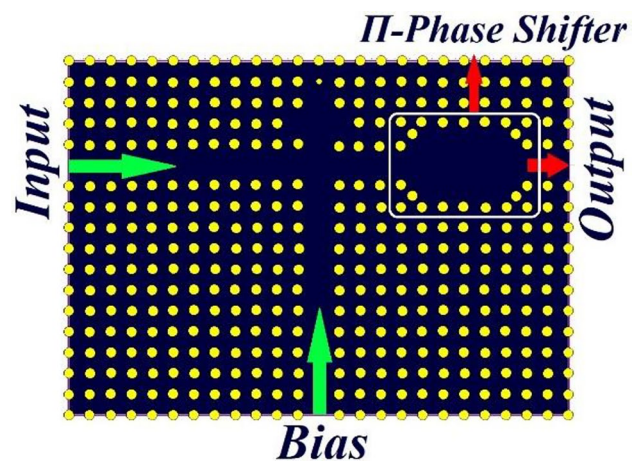

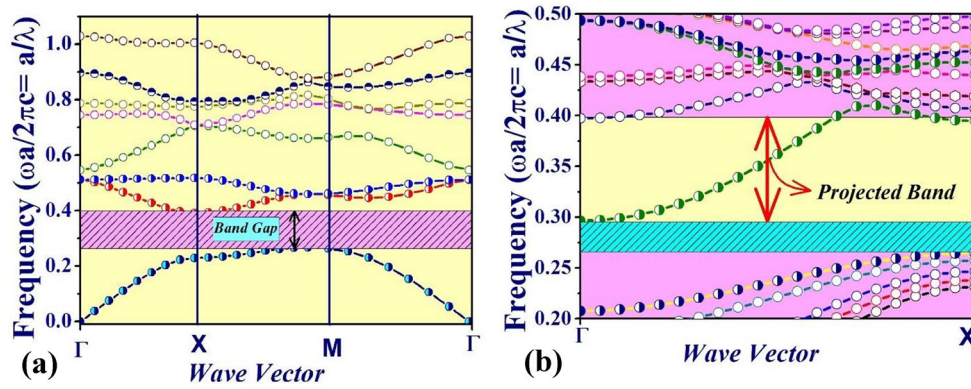**Fig. 1** Two-dimensional schematic representation of proposed optical isolator

Fig. 2 (**a**) Band diagram representation of non-defect PhC. (**b**) Guided band diagram representation of defect mode PhC

has been introduced in the horizontal waveguide (right side of the junction) by removing three rods from both the sides of the waveguide and four corner rods of the phase shifter unit have been shifted away from the waveguide by period/2 in Γ-M direction (diagonally). Additionally, to control the propagation of bias signal, a cavity has been created at the top of the junction by removing four rods and diameter of a rod (which is placed at the top portion of the cavity) is optimized as 90 nm as shown in Fig. 1.

Applying plane wave expansion (PWE) algorithm [51], the band diagram of the non-defect PhC structure has been calculated, which is shown in Fig. 2a. It is observed from Fig. 2a that the complete photonic band gap (PBG) is found in transverse magnetic (TM) mode with the normalized frequency of 0.26 to 0.4 a/λ which are equivalent to the wavelength range 1350 to 2076 nm. No such band gap has been obtained in transverse electric (TE) mode. Similarly, the projected band analysis of the PhC in defect mode has also been done by applying PWE algorithm, as shown in Fig. 2b. From Fig. 2b, it is noticed that the guided band of the defect

mode of the PhC exhibits (in TM mode) almost within the entire photonic band gap.

3 Simulation Results and Performance Analysis

The simulation of the proposed device has been carried out by using finite difference time domain (FDTD) [52] method to analyze the electric field distribution within the waveguide. A monochromatic continuous wave (CW) of normalized frequency 0.349 (a/λ) (equal to 1550 nm wavelength) is used to operate the device. The unidirectional function of the proposed device has been realized by introducing the π-phase shifter and the cavity within the waveguide. A CW optical signal with half of unity power has been applied at the bias port to make interference with the signal coming from input/output ports of the device. Three possible operating conditions of the proposed isolator are discussed as follows:
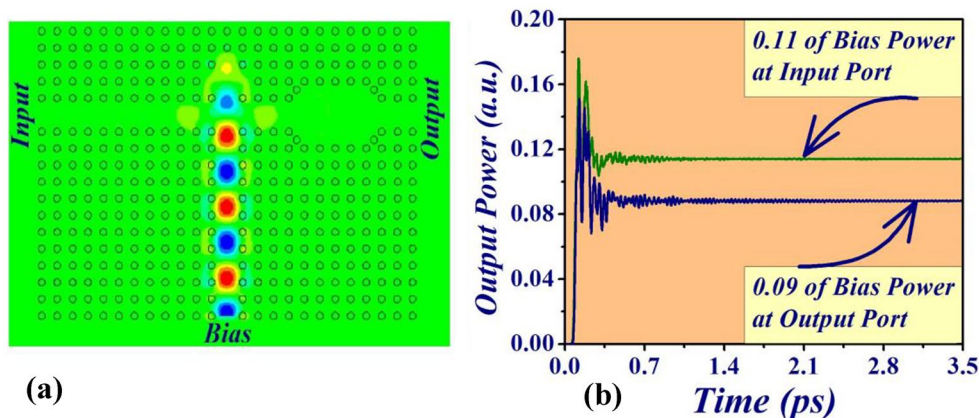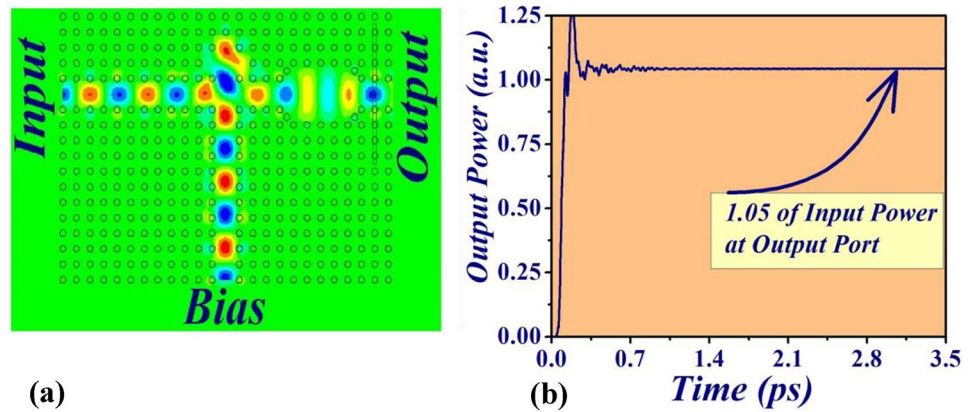

Fig. 3 (**a**) Electric field propagation profile through the waveguides. (**b**) Graphical representation of TM signal power, when only bias signal is applied in the device

Fig. 4 (**a**) Electric field propagation profile within the waveguides. (**b**) Graphical representation of TM signal propagation, when signal is applied at the input port along with bias signal

For the first case, only a Gaussian TM-polarized optical signal (bias) is launched at the bias input as shown in Fig. 3a. The amplitude and phase of the signal are considered as 0.5Pi (where Pi is considered as power of input signal) and 0, respectively. It can be seen from Fig. 3a that when only CW bias signal is applied, it is directed toward the cavity at the top of the structure. A portion of the bias signal is then reflected back from the cavity, which is directed toward bias input ports. As a result, the destructive interference occurs at the junction between forward propagating bias signal and backward propagating bias signal. Therefore, negligible amount of signal 0.11Pi and 0.09Pi powers (11% and 9%) appeared at input port and output port, respectively, which is shown in Fig. 3b.

Secondly, a monochromatic continuous wave (CW) with unity signal power excited to the input port along with bias signal. In Fig. 4a, the corresponding electric field propagation profile is shown, which shows that at junction, the signal from the bias meets with input signal and makes constructive interference as they are on same phase. The signal power at the output port has been calculated as 1.05Pi, as shown in Fig. 4b. This signifies that, during forward propagation, the proposed isolator provides substantial high optical power at the output port.

Finally, the schematic illustration of the state in which optical signal is applied from output terminals is depicted in Fig. 5. When the optical signal passes through the π-phase shifter, it changes the phase by 180 degrees of the signal. From Fig. 5a, it can be viewed that, after passing through the π-phase shifter, it reaches the junction and meets with bias signal with out-of-phase which occurs destructive interference between them. As a result, a negligible optical power of 0.09Po (where Po is considered as signal power is applied at the output port) appeared at the input port as shown in Fig. 5b. This signifies that, during backward propagation, the proposed isolator provides negligibly low optical power at the input port.

The results of the simulation are summarized in Table 1, where three different working states for the proposed structure have been considered. When only bias signal is ON, the output port as well as input port is OFF and signal power at the output and input are 0.09Pi and 0.11Pi. When input is ON, then the output power is 1.05Pi which implies that output is ON. At last, when signal is applied at output port, then the input power is 0.09Po which is considered as OFF. Comparing these results with the truth table of isolator/diode confirms that the proposed structure can be operated as an all-optical isolator. However, several performance

Fig. 5 (**a**) Electric field propagation profile within the waveguides. (**b**) Graphical representation of TM signal propagation, when signal is applied at the output port along with bias signal
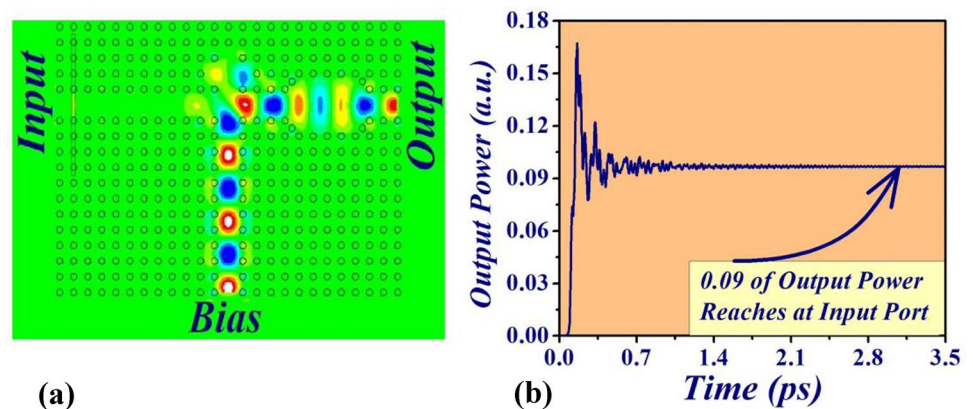
Table 1 Input/output power and logic level representation

Input operating conditions			Output condition	
Bias	Input	Output	Input	Output
0.5 (ON)	0 (OFF)	0 (OFF)	0.11Pi (OFF)	0.09Pi (OFF)
0.5 (ON)	1Pi (ON)	0 (OFF)	—–	1.05Pi (ON)
0.5 (ON)	0 (OFF)	1Po (ON)	0.09Po (OFF)	—–

parameters of the proposed isolator have been analyzed, which are discussed in the subsequent subsections.

3.1 Power Variation

In case of forward propagation of the proposed device, the signal power has been measured at the output port. Initially, the power of bias signal has been fixed as half of unity power (0.5Pi), then the signal power at the input port has been varied from null (0Pi) to 1.5Pi, as shown in Fig. 6. Very interesting phenomenon has been observed while determining the output power by increasing the input power from 0 to 1.5Pi that the power at the output port increases/decreases with equal proportion of the input signal. For example, if half of unity power (0.5Pi) is applied at the input port, then approximately same amount of power is received at the output port. Therefore, from this observation, it can be concluded that the power of bias signal does not affect the power level of the output signal.

3.2 Transmittance

The transmittance of the proposed isolator has also been calculated for both the operating conditions, which are depicted in Fig. 7. Transmittance of an optical device/switch is considered as the obtained output power with respect to various input wavelengths. In Fig. 7a, the transmittance of the device at the output port (forward propagation) has been shown with input signal wavelength range of 1200 to 1800 nm. It is observed from the figure that the maximum transmittance
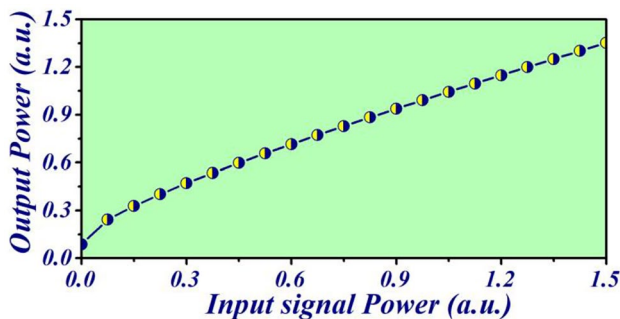
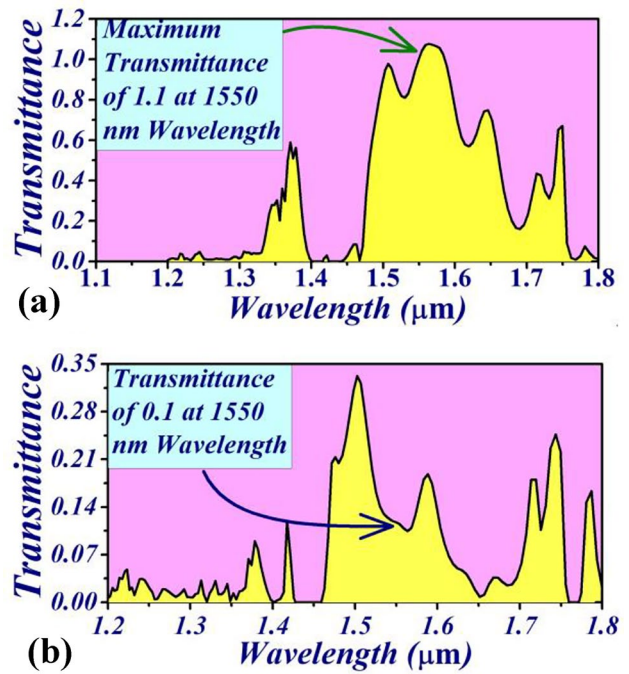**Fig. 6** Change of output power with respect to input power

Fig. 7 Transmittance of proposed isolator at (**a**) forward propagation condition and (**b**) backward propagation condition

is obtained at 1550 nm wavelength. Moreover, Fig. 7a shows that the proposed device exhibits approximately unity transmission in forward propagation in the range of 1530 to 1580 nm of input signals. Therefore, this signifies that the proposed device offers the bandwidth of ~ 6.2 THz.

On the other hand, the transmittance characteristics of backward propagation of the proposed device have also been analyzed. Figure 7b depicts that the transmittance of 0.1 has achieved at 1550 nm wavelength. Moreover, from Fig. 7b, it is observed that in backward propagation, the proposed device also offers substantial low transmittance in the range of 1530 to 1580 nm of input signals. Therefore, the above analysis of the device proves that the proposed device offers a wide bandwidth of ~ 6.2THz (with center wavelength of 1550 nm) for the propagation of both directions.

3.3 Contrast Ratio

The contrast ratio is one of the crucial parameters for examining the performance of the device. The noise margin of a device is directly proportional to the contrast ratio whereas bit error rate (BER) is inversely proportional to it. Hence, the channel performance of the device would be improved by increasing contrast ratio. Therefore, for better performance of the device, always a high contrast ratio is expected. The definition of contrast ratio is considered as a ratio between the power at ON state (logic-1) and OFF state (logic-0). Mathematically, the contrast ratio is expressed as follows:

$$Contrast\ Ratio = 10\log\frac{P_1}{P_0}$$

where $P1$ is considered as signal power level at ON state and $P0$ is considered as the signal power levels at OFF state.

ON state and OFF state power levels of the device have been measured and tabulated in Table 1 as 1.05Pi and 0.09Pi, respectively. By applying the above expression, the contrast ratio of the device has been calculated as ~ 10 dB.

3.4 Comparative Study

Table 2 is organized to present a comparison between some previously reported optical isolators with the proposed one. The comparison encompasses different types of materials/platforms, including PhC, which have been used for designing isolators. Attributes for the comparison are considered as whether the model operates on the principle of linear or nonlinear optics, footprint of the design, minimum (threshold) power required for operation, contrast (isolation) ratio between the powers of the states of the output, and the transmittance at the allowed states. The first two entries in the table [44, 53] are reports where MZIs, phase modulator, polarizer, and/or sampler has been used to design isolators. Although these designs offer significantly high contrast ratio, the optical components used in these designs are having large footprint (in the range of millimeters). Hence, these designs are not suitable for dense integration in PICs. On the other hand, spin-Hall effect of light in Ce:YIG film-based magneto optic material has been used in [54] to design an isolator that provides a contrast ratio of 20 dB. Also, polariton graphene-based topological optical isolator has been designed in [55], which gives a tremendous contrast ratio, i.e., 49 dB. However, in spite of their fabulous performance, integration of these devices in silicon photonic-based PICs becomes quite challenging due to the typicality of the used materials. In contrast, compared to the aforesaid

Table 2 Comparative report on some optical isolator

Ref	Platform/material used	Linear/nonlinear	Principle/topology/tool adopted	Footprint	Threshold Power	Contrast Ratio	Transmission
[44]	Bismuth, lutetium, and neodymium-iron garnet film on GGG substrate	Linear	Nonreciprocal interference using Mach–Zehnder interferometer	8 mm long waveguide, 24.4um arm separation	——	19 dB	—-
[53]	Indium phosphide (InP) substrate	Nonlinear	Two-phase modulators in series	800um × 2.06 mm (approx)	—-	11 dB (Isolation)	—-
[54]	Ce: YIG film	——	Spin-Hall effect of light	——	——	20 dB (isolation ratio)	—-
[55]	Polaritongraphene lattice	—–-	Quantum anomalous Hall effect	40 μm long	—-	49 dB (isolation ratio)	——
[47]	PhC (rods-in-air)	Nonlinear	Asymmetric PhC L-shaped waveguide with a single nonlinear microcavity	30 μm^2 (approx)	—-	—	90% (forward transmission)
[46]	PhC (rods-in-air)	Nonlinear	Nonlinear ring resonators	24 × 24 matrix	2.69GW/cm^2	57% contrast	—-
[56]	PhC (rods-in-air)	Nonlinear	Asymmetric coupling by Fano-cavity and F–P cavity	10 × 18 matrix	0.5mW/μm	—-	Above 90% (forward transmission)
[57]	Heterostructure PhC lattice containing rectangular metals and air holes	Linear	Directional band gap mismatch/the self-collimation effect	21 μm^2 (approx)	—-	28 dB (approx)	60% forward transmission, 0.1% backward transmission
This Work	PhC (rods-in-air)	Linear	Light beam interference	131 μm^2	——	10 dB (contrast ratio)	——

designs, PhC-based designs are much simpler to integrate with PICs using the very same CMOS fabrication process technologies that are used to design silicon-based photonic and electronic devices. Thereby, PhC-based components, aided by their inherent abilities to control optical signals in sub-wavelength scale, have been observed to play important role in PIC design. Also, in the present context, linear and nonlinear optical interactions in PhCs have been used for designing isolators. Some nonlinear PhC-based designs [47, 56] have been seen to provide very high forward transmission, and the size of the devices is significantly small as well. However, high input power (threshold power) is needed for proper functioning of a nonlinear device. On the contrary, one linear optical phenomena-based isolator model [57], whose operations are not constrained by a threshold power, have been designed within small footprint areas. But the forward transmittances in the design are insufficient and, hence, incur a huge loss when integrated in a PIC. Moreover, most of the designs are purely two dimensional; i.e., the third dimension (normal to the plane of the periodicity of the crystal) is considered as indefinitely extended, which is quite impractical. On the other hand, the proposed isolator is designed in a 3D PhC platform considering all the abovementioned facts, such that concern of practicality gets alleviated. Moreover, the linear optics-based operational regime of the proposed isolator removes the requirement of any threshold power. Not the least, the reasonably good isolation (contrast ratio) and small footprint of the isolator keep it ahead of several designs in the context of its integration to silicon-based PICs.

4 3-Dimensional Design and Analysis of 3D-FDTD Simulation

A physical device should have finite values in all the three directions. Thereafter, the performance of proposed optical isolator has also been analyzed with a finite slab height of 5 μm. The 3-dimensional design of the device is shown in Fig. 8, where the height of all the rods has been chosen 3 μm. All these rods (3 μm) are having three layers, where each top

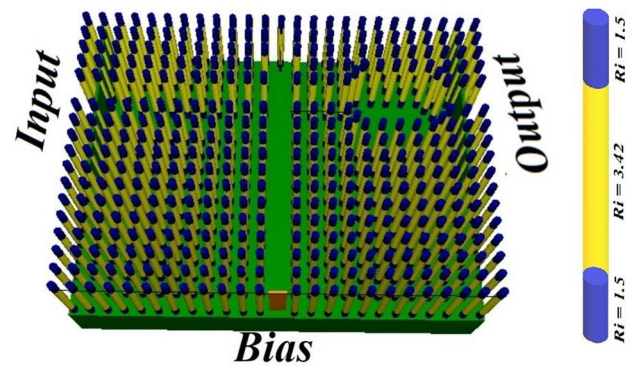**Fig. 8** Schematic representation of proposed device in 3-dimenssional finite slab height

and bottom layers of each rods are 0.5 μm (500 nm) long and the middle layer is 2 μm long. To maintain the vertical symmetry of refractive index of the photonic crystal slab, the refractive index profile of all three layers of each rods has been into consideration. The top and bottom layers of a rod are having refractive index of 1.5 whereas the middle layer has refractive index of 3.42. Moreover, to make the device mechanically stable, all the multilayer rods are placed on a silica slab (SiO2), of refractive index 1.5 with a thickness of 2 μm.

3D-FDTD algorithm has been applied to observe the electric field propagation profile and to analyze the performances of the device. Propagation profiles of the device for different input combination, such as no input condition, forward propagation, and backward propagation of the device, are chronologically depicted in Figs. 9–11. Figure 9 depicts the electric field propagation profile of the device when only bias signal is applied. From Fig. 9b, it is observed that only 12% and 10% of unit powers appeared at the input and output port, respectively, which are almost equal compared to their two-dimensional simulation counterpart. The simulation result also helps to calculate the steady-state time of the proposed device. Moreover, the simulation result has also been analyzed when monochromatic (1550 nm wavelength) CW is applied at the input port along with bias signal as shown in

Fig. 9 (a) Electric field propagation profile through the waveguides. (b) Graphical representation of TM signal power, when only bias signal is applied in the device with finite slab height structure
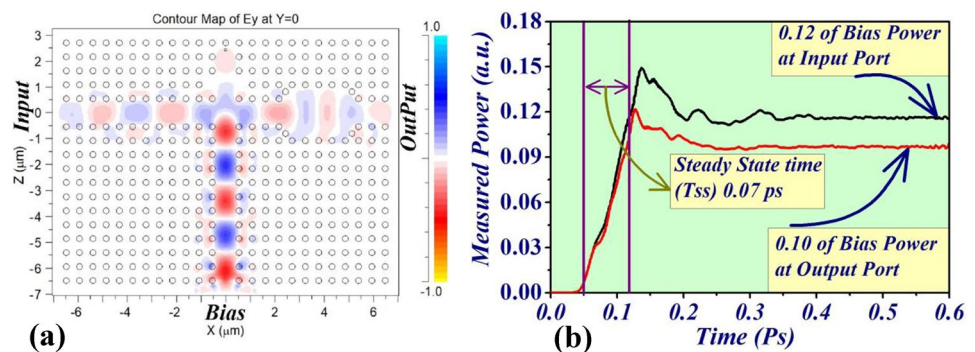
Fig. 10 (a) Electric field propagation profile within the waveguides. (b) Graphical representation of TM signal propagation, when signal is applied at the input port along with bias signal in finite slab height structure
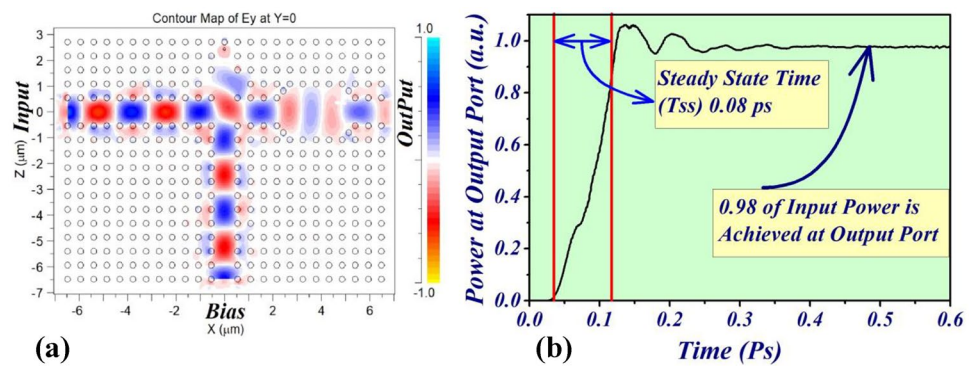

Fig. 11 (a) Electric field propagation profile within the waveguides. (b) Graphical representation of TM signal propagation, when signal is applied at the output port along with bias signal in finite slab height structure
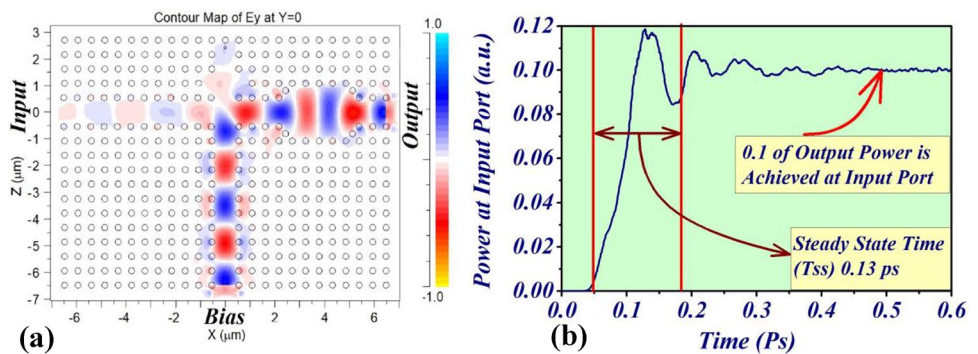

Fig. 10. From Fig. 10b, it is observed that in forward propagation, the device delivers approximately unit power at the output port. Finally, the monochromatic continuous optical signal is applied at output terminal along with bias signal. The electric field propagation profile of the same is depicted in Fig. 11. The Fig. 11b shows that in backward propagation, almost negligible amount of optical power arrives at the input port. The 3D-FDTD simulation results, for three different combinations, prove that the signal powers are obtained at desired output ports in 3D structure of the device which are equal compare to its 2D simulation counterpart. Therefore, the above 3D simulations prove that the proposed device is practicable for future generation photonic application.

Nevertheless, the CMOS fabrication procedure has become matured enough; therefore, the fabrication of this structure has now become feasible. Although there are several techniques for fabrication of PhC structures, the process technology for the proposed multilayer 2D PhC rods-in-air structure may be realized following the similar procedures as described in [58–61]. The process can be generalized as follows.

- Generation of SiO_2 layer (bottom layer) on silicon wafer by oxidation.
- Deposition of Si layer (middle layer) by MBE/PECVD.
- Deposition of photoresist for patterning.

- Sputter deposition of SiO_2 layer (top layer).
- Deposition of photoresist.
- Definition of the design (PhC structures) using e-beam lithography followed by development and lift-off.
- Etching of the structures using RIE/DRIE.
- Resist ashing and cleaning.

5 Conclusion

In this paper, a new design of all optical isolator has been proposed in 2D silicon square lattice of rods in air structure. The operating principle of the device is based on optical beam interference. The device has been designed for the standard wavelength of optical communication, i.e., 1.55 μm. In the worst case, the device is capable to offer a contrast ratio of 10 dB. Moreover, the device provides a substantial high bandwidth of ~ 6.2 THz around 1.55 μm optical wavelength. The 3-dimenssional structure of the device has also been designed and the performances have been evaluated, which is almost similar to its 2-dimensional counterpart. The 3D simulation results indicate that this device is suitable for next-generation optical chip design.

Declarations

Conflict of Interest The authors declare no competing interests.

References

1. T. Ladd, F. Jelezko, R. Laflamme, Y. Nakamura, C. Monroe, J.L. O'Brien, Quantum computers. Nature **464**, 45–53 (2010)

2. A. Vahdat, H. Liu, X. Zhao, C. Johnson, The emerging optical data center, Optical Fiber Communication Conference/National Fiber Optic Engineers Conference 2011, paper OTuH2 (2011)

3. S. Minardi, R.J. Harris, L. Labadie, Astro-photonics: Astronomy and modern optics, Astron. Astrophys. Rev. **29**(6), (2021)

4. P.B. Reid, W. Davis, D.A. Schwartz, S. T-McKinstry, R.H.T Wilke, Technology challenges of active x-ray optics for astronomy, Proc. SPIE 7803, Adaptive X-Ray Optics, **7803**(78030I), (2010)

5. C.V. Poulton, M.J. Byrd, P. Russo, E. Timurdogan, M. Khandaker, D. Vermeulen, M.R. Watts, Long-range LiDAR and free-space data communication with high-performance optical phased arrays. IEEE J. Sel. Top. Quantum Electron. **25**(5), 1–8 (2019)

6. C. Rablau, LIDAR – A new (self-driving) vehicle for introducing optics to broader engineering and non-engineering audiences, Fifteenth Conference on Education and Training in Optics and Photonics, **11143**(138), (2019)

7. E. Yablonovitch, Inhibited spontaneous emission in solid-state physics and electronics. Phys. Rev. Lett. **58**, 2059–2062 (1987)

8. M.A. Baqir, A. Farmani, T. Fatima, M.R. Raza, S.F. Shaukat, A. Mir, Nanoscale, tunable, and highly sensitive biosensor utilizing hyperbolic metamaterials in the near-infrared range. Appl. Opt. **7**(31), 9447–9454 (2018)

9. A. Alipore, A. Farmani, A. Mir, High sensitivity and tunable nanoscale sensor based on plasmon-induced transparency in plasmonic metasurface. IEEE Sens. J. **18**(17), 7047–7054 (2018)

10. G.D. Hutcheson, Moore's law, lithography, and how optics drive the semiconductor industry, Proc. SPIE, Extreme Ultraviolet (EUV) Lithography IX, **10583**(03), (2018)

11. H. Radamson, L. Thylén, Chapter 4 - Moore's law for photonics and electronics, Monolithic nanoscale photonics–electronics integration in silicon and other group IV elements, pp. 121–150 (2015)

12. C. Xue, W. Dengkui, W. Tuo et al., Enhanced photoresponsivity of a GaAs nanowire metal-semiconductor-metal photodetector by adjusting the fermi level. ACS Appl. Mater. Interfaces **11**(36), 33188–33193 (2019)

13. H. Li, J. Tang, Y. Kang, et al., Optical properties of quasi-type-II structure in GaAs/GaAsSb/GaAs coaxial single quantum-well nanowires, Appl. Phys. Lett. **113**, 233104 (2018)

14. X. Zhang, Y. Tang, F. Zhang, C. Lee, A novel aluminum–graphite dual-ion battery. Adv. Energy Mater. **6**(11), 1502588 (2016)

15. X. Xu, M. Nieto-Vesperinas, Azimuthal imaginary Poynting momentum density, Phys. Rev. Lett. **123**, 233902 (2019)

16. Shun Lien Chuang, Physics of Photonic Devices, 2nd Edition, Wiley, ISBN: 978-0-470-29319-5, January (2009)

17. F. Parandin, M. M Karkhanehchi, M. Naseri A. Zahedi, Design of a high bitrate optical decoder based on photonic crystals, J. Comput. Electron. **17**(2), (2018)

18. H. A. Banaei, M. G. Rabati, P. A Badelbou F. Mehdizadeh, Effect of self-collimated beams on the operation of photonic crystal decoders, J. Electromagn. Waves. Appl. **30**(11), 1440–1448 (2016)

19. K. Goswami, H. Mondal, M. Sen, Optimized design of 60° bend in optical waveguide for efficient power transfer, In: Bera R., Pradhan P.C., Liu CM., Dhar S., Sur S.N. (eds) Advances in Communication, Devices and Networking, Lecture Notes in Electrical Engineering **662**, Springer, (2020)

20. A. Farmani, A. Mir, M. Irannejad, 2D-FDTD simulation of ultra-compact multifunctional logic gates with nonlinear photonic crystal. J. Opt. Soc. Am. B. **36**(4), 811–818 (2019)

21. M.J. Maleki, A. Mir, M. Soroosh, Ultra-fast all-optical full-adder based on nonlinear photonic crystal resonant cavities. Photon. NetwCommun. **41**, 93–101 (2021)

22. H.P. Mondal, M. Sen, C. Prakash, K. Goswami, C. Sarma, Impedance matching theory to design all-optical AND gate. IET Optoelectron. **12**(4), 244–248 (2018)

23. K. Goswami, H.P. Mondal, P. Das, A. Thakuria, Realization of ultra-compact all-optical logic AND gate based on photonic crystal waveguide, ICCDN 2021. Lect. Notes Electr. Eng. **776**, 61–68 (2022)

24. H.P. Mondal, S. Chanda, P. Gogoi, Realization of all-optical logic AND gate using dual ring resonator, IEEE international conference on automatic control and dynamic optimization technique (ICACDOT-2016), 553–556 (2016)

25. H.P. Mondal, S. Chanda, M. Sen, T. Datta, All-optical AND gate based on silicon photonic crystal, IEEE International Conference on Microwave and Photonics, Indian School of Mines, Dhanbad, Jharkhand, 1–2 (2015)

26. H.P. Mondal, K. Goswami, M. Sen, C. Prakash, An all-optical ultra-compact 4-channel wavelength de-multiplexer, IEEE International Conference on Microwave and Photonics, Indian School of Mines, Dhanbad, Jharkhand, (2018)

27. D. Gogoi, K. Das, H. P. Mondal, P. Talukdar, K. Hussain, Design of ultra-compact 3-channel wavelength de-multiplexer based on photonic crystal, IEEE international conference on automatic control and dynamic optimization technique (ICACDOT-2016), I2IT, Pune, Maharashtra, (2016)

28. M.J. Maleki, M. Soroosh, A. Mir, Improving the performance of 2-to-4 optical decoders based on photonic crystal structures, Crystals **9** (12), 2019

29. T. Daghooghi, M. Soroosh, K. Ansari-Asl, Ultra-fast all-optical decoder based on nonlinear photonic crystal ring resonators. Appl. Opt. **57**, 2250–2257 (2018)

30. H.P. Mondal, M. Sen, K. Goswami, Design and analysis of all-optical 1-to-2-line decoder based on linear photonic crystal. IET Optoelectron. **13**(4), 191–195 (2019)

31. F. Mehdizadeh, M. Soroosh, H.A. Banaei, A novel proposal for optical decoder switch based on photonic crystal ring resonators, Opt. Quantum Electron. **48**(20), (2016)

32. T. Daghooghi, M. Soroosh, K. Ansari-Asl, A low-power all optical decoder based on photonic crystal nonlinear ring resonators. Optik **174**, 400–408 (2018)

33. A. Sharma, K. Goswami, H. Mondal et al., A review on photonic crystal based all-optical logic decoder: linear and nonlinear perspectives. Opt. Quant. Electron. **54**, 90 (2022)

34. H.P. Mondal, M. Sen, K. Goswami, Design, and analysis of a 0.9Tb/s 6-channel WDM filter based on photonic crystal waveguides, J. Opt. Soc. Am. B. **36**(11), 3181–3188 (2019)

35. C. Prakash, M. Sen, H.P. Mondal, K. Goswami, Design and optimization of a slotted-PhC waveguide based TE-pass polarization filter. J. Opt. Soc. Am. B. **35**(8), 1791–1798 (2018)

36. C. Prakash, H.P. Mondal, K. Goswami, M. Sen, Investigation for the efficient interface of strip and PhC Slot waveguide, IEEE International Conference on Microwave and Photonics, Indian School of Mines, Dhanbad, Jharkhand, (2018)

37. R.R. Ghosh, T. Datta, H.P. Mondal, M. Sen, Efficient TE-pass polarizer based on photonic crystal slot waveguide, International Conference on Opto-Electronics and Photonic Materials, SASTRA University, Thanjavur, Tamilnadu, (2015)

38. K. Goswami, H.P. Mondal, M. Sen, A review on all-optical logic adder: Heading towards next-generation processor, Opt. Commun. **483**, 126668 (2020)

39. M.M. Karkhanehchi, F. Parandin, A. Zahedi, Design of an all-optical half-adder based on 2D photonic crystals. Photon. Netw. Commun. **33**, 159–165 (2017)

40. S. Serajmohammadi, H.A. Banaei, F. Mehdizadeh, Proposal for realizing an all-optical half adder based on photonic crystals. Appl. Opt. **57**, 1617–1621 (2018)

41. F. Parandin, M.R. Malmir, M. Naseri, All-optical half-subtractor with low-time delay based on two-dimensional photonic crystals. Superlattices Microstruct. **109**, 437–441 (2017)

42. C.R. Doerr, N. Dupuis, L. Zhang, Optical isolator using two tandem phase modulators. Opt. Lett. **36**(21), 4293–4295 (2011)

43. S. Hua, J. Wen, X. Jiang, Q. Hua, L. Jiang, M. Xiao, Demonstration of a chip-based optical isolator with parametric amplification. Nature Communication **7**, 13657 (2016)

44. J. Fujita, M. Levy, R.M. Osgood Jr., Waveguide optical isolator based on Mach–Zehnder interferometer, Appl. Phys. Lett. **76**(16), (2000)

45. O. Zhuromskyy, M. Lohmeyer, N. Bahlmann, H. Dotsch, P. Hertel, A.F. Popkov, Analysis of polarization independent Mach-Zehnder-type integrated optical isolator. J. Lightwave Technol. **17**(7), 1200–1205 (1999)

46. P.K. Sahoo, J. Joseph, Optical diode using nonlinear polystyrene ring resonators in two-dimensional photonic crystal structure. Appl. Opt. **52**, 8252–8257 (2013)

47. E.N. Bulgakov, A.F. Sadreev, All-optical diode based on dipole modes of Kerr microcavity in asymmetric L-shaped photonic crystal waveguide. Opt. Lett. **39**(7), 1787–1790 (2014)

48. A. Rostami, Piecewise linear integrated optical device as an optical isolator using two-port nonlinear ring resonators. Opt. Laser Technol. **39**(5), 1059–1065 (2007)

49. C. Wang, C.-Z. Zhou, Z.-Y. Li, On-chip optical diode based on silicon photonic crystal heterojunctions. Optical Express **19**(27), 26948–26955 (2011)

50. E. Shaik, N. Rangaswamy, Implementation of photonic crystal based all optical half adder using T-shaped waveguides, Second International Conference on Computing and Communications Technologies, India, 148–150 (2017)

51. S.G. Johnson, J.D. Joannopoulos, Block-iterative frequency domain methods for Maxwell's equations in a plane wave basis. Opt. Express **8**, 173–190 (2001)

52. W.P. Huang, S.T. Chu, S.K. Chaudhuri, A semi-vectorial finite-difference time-domain method (optical guided structure simulation). IEEE Photonics Technol. Lett. **3**(9), 803–806 (1991)

53. C.R. Doerr, N. Dupuis, L. Zhang, Optical isolator using two tandem phase modulators, Opt. Lett. **36**(21), (2011)

54. Y. Kawaguchi, M. Li, K. Chen, V. Menon, et al., Optical isolator based on chiral light-matter interactions in a ring resonator integrating a dichroic magneto-optical material, Appl. Phys. Lett. (2021)

55. D.D. Solnyshkov, O. Bleu, G. Malpuech, Topological optical isolator based on polariton graphene, Appl. Phys. Lett. **112**, (2018)

56. B. Liu, Y. Liu, S. Li, X. He, High efficiency all-optical diode based on photonic crystal waveguide. Opt. Commun. **368**, 7–11 (2016)

57. S. Feng, C. Ren, W. Wang, Y. Wang, All-optical diode based on the self-collimation characteristics of the near-infrared photonic crystal heterojunctions, EPL, (2012)

58. P. Bienstman, S. Assefa, S.G. Johnson, J.D. Joannopoulos, G.S. Petrich, L.A. Kolodziejski, Taper structures for coupling into photonic crystal slab waveguides. J. Opt. Soc. Am. B. **20**(9), 1817–1821 (2003)

59. S. Assefa, P.T. Rakich, P. Bienstman, S.G. Johnson, G.S. Petrich, J.D. Joannopoulos, L.A. Kolodziejski, E.P. Ippen, Henry I. Smith, Guiding 1.5 µm light in photonic crystals based on dielectric rods, Appl. Phys. Lett. **85**(25), (2004)

60. T-M. Shih, A. Kurs, M. Dahlem, G. Petrich, M. Soljačić, E. Ippen, L. Kolodziejski, K. Hall, M. Kesler, Supercollimation in photonic crystals composed of silicon rods, Appl. Phys. Lett. **93**(13), (2008)

61. A.A.M. Kok, C.M. Heesch, van, E.J. Geluk, M.J.H. Sander - Jochem, J.J.G.M. Tol, van der, Y.S. Oei, M.K. Smit, Two-dimensional photonic crystals based on InP rods, proc. CNM Research Day, Eindhoven, conference, CNM Research Day, (2006)